applied optics

Automated batch characterization of inkjet-printed elastomer lenses using a LEGO platform

Yu-Lung Sung,[1] Jacob Garan,[2] Hoang Nguyen,[1] Zhenyu Hu,[1] and Wei-Chuan Shih[1,3,4,5,*]

[1]Department of Electrical and Computer Engineering, University of Houston, 4800 Calhoun Rd., Houston, Texas 77004, USA
[2]College of Optical Sciences, University of Arizona, 1401 East University Boulevard, Tucson, Arizona 85721, USA
[3]Department of Biomedical Engineering, University of Houston, Houston, Texas 77004, USA
[4]Department of Chemistry, University of Houston, Houston, Texas 77004, USA
[5]Program of Materials Science and Engineering, University of Houston, Houston, Texas 77004, USA
*Corresponding author: wshih@uh.edu

Received 12 June 2017; revised 5 August 2017; accepted 9 August 2017; posted 10 August 2017 (Doc. ID 297793); published 7 September 2017

Small, self-adhesive, inkjet-printed elastomer lenses have enabled smartphone cameras to image and resolve microscopic objects. However, the performance of different lenses within a batch is affected by hard-to-control environmental variables. We present a cost-effective platform to perform automated batch characterization of 300 lens units simultaneously for quality inspection. The system was designed and configured with LEGO bricks, 3D printed parts, and a digital camera. The scheme presented here may become the basis of a high-throughput, in-line inspection tool for quality control purposes and can also be employed for optimization of the manufacturing process.

OCIS codes: (080.0080) Geometric optics; (110.0110) Imaging systems; (180.0180) Microscopy; (150.0150) Machine vision.

https://doi.org/10.1364/AO.56.007346

1. INTRODUCTION

Recent advances in inkjet-printed optics have created a new class of lens fabrication technique: lenses with tunable geometry, focal length, and magnification can be fabricated by curing controlled amounts of liquid elastomer on a heated surface. This fabrication technique is cost effective and scalable and can produce an optically smooth surface. The resulting small, self-adhesive lens can be attached onto a smartphone camera, similar to wearing a contact lens, and enables smartphones to achieve a spatial resolution approaching 1 μm. The lens curvature modifies the optical path to the imaging sensor and enables a working distance as short as 2 mm [1]. The increasingly popular field of smartphone microscopy has shown great potential in mobile point-of-care diagnostic systems, particularly for histology of tissue sections and cytology of blood cells [2]. Self-adhesive, single-lens-based microscopy represents an innovative approach fundamentally different from other more complex smartphone microscopes [3].

Compared with lenses made of hard materials, such as glass and plastics by grinding [4] or molding, [5], inkjet printing represents a new concept of lens formation. However, due to the free surface formation process, changes in environmental factors during fabrication may result in dimensional variations across lenses [6]. In particular, the diameter and focal length of a lens are key parameters that dictate its magnification and imaging performance and thus require detailed individual characterization.

Existing lens inspection protocols often involve random lens sampling [7], surface profiling with tools such as a profilometer or lensometer [8], and manual observations for scratches or blemishes [9]. Existing microlens characterization protocols rely on exhaustive cleaning and verification of the master lens mold [10] and interference microscopy of a random sampling of the manufactured array [11]. The measurement of lens diameter and focal length can be time consuming if performed individually. Furthermore, the flexible materials used to print the lens may deform when mechanical measurements are performed. A new lens characterization platform is needed to fully exploit the low-cost, parallel inkjet-printing process.

Imaging systems have been widely used for quality control in production-line manufacturing, particularly to inspect for microscopic imperfections of lathed and machined components. These systems are typically incorporated into custom-made quality control installations that are only financially feasible for large-scale productions. In contrast, low-cost imaging systems built on standardized components, such as LEGO bricks have been explored in the past to create versatile optical systems [12–16]. To implement an inexpensive, simple, and fast inspection scheme, here we utilize LEGO bricks, 3D printed parts, and a camera with a laptop to create a lens characterization system. The system employs parallel imaging of a

large number of lenses (up to 300) and extracts key parameters by automated computer analysis.

2. LENS PRINTING SETUP

A lens array was printed using an elastomer curing technique [1] on a glass substrate (20 cm × 20 cm). The lens geometry is controlled by factors such as the substrate temperature and elastomer volume. For example, a previously reported parameter set involved individual droplets of 50 μL ± 0.1% and a glass substrate temperature at 200°C. However, the accuracy of variables such as surface temperature is hard to guarantee over large printing areas. Equipment quality and flatness issues introduce small variations that may detrimentally affect desired specifications. For example, an infrared heat map of a lens array immediately after the printing process confirms a non-uniform temperature distribution (obtained with FLIR A300), as shown in Fig. 1(a). The resulting lenses shown in Figs. 1(b)–1(d) are selected from regions of different temperatures (185, 200, and 215°C) and have correspondingly different diameters (6.55, 6.10, and 5.80 mm).

To accurately characterize the imaging resolution afforded by a single lens, the lens was attached to a smartphone camera (Lumia 640) with a built-in camera module consisting of a $f/2.2$ lens and a 6.35 mm (1/4 inch diagonal or 5.08 mm × 3.81 mm) 8-megapixel (3264 × 2448 pixels) CMOS imaging sensor. A USAF 1951 resolution test target was imaged to obtain the minimum resolvable distances, which were found to be 35, 10, and 9 μm for the lenses printed at 185, 200, and 215°C, respectively [Figs. 1(e)–1(g)]. Such variation within one batch warrants each lens to be characterized; however, the procedure of checking the magnification and resolution of each lens through direct test-target imaging is time consuming and prone to human error. The goal of this work is therefore to measure lens parameters simultaneously from multiple lenses and relate them to system magnification and resolution without direct test-target imaging.

3. CHARACTERIZATION SETUP

The lens characterization setup was built with LEGO components (bricks, gears, and motors), 3D printed parts, a Fresnel lens, and two flat mirrors. The printed lens array was inserted into a holder in the light path, as shown in Fig. 2. For focal length characterization, the lens array was illuminated by a

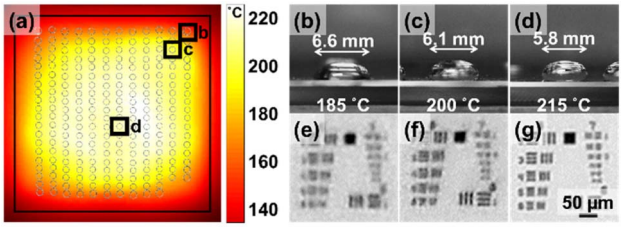

Fig. 1. (a) Printed lens array overlaid with temperature distribution map. (b)–(d) Three different lens diameters with corresponding printing temperatures. (e)–(g) Minimum resolvable features measured to be 35, 10, and 9 μm corresponding to lenses in (b)–(d), respectively, using a USAF 1951 resolution test target.

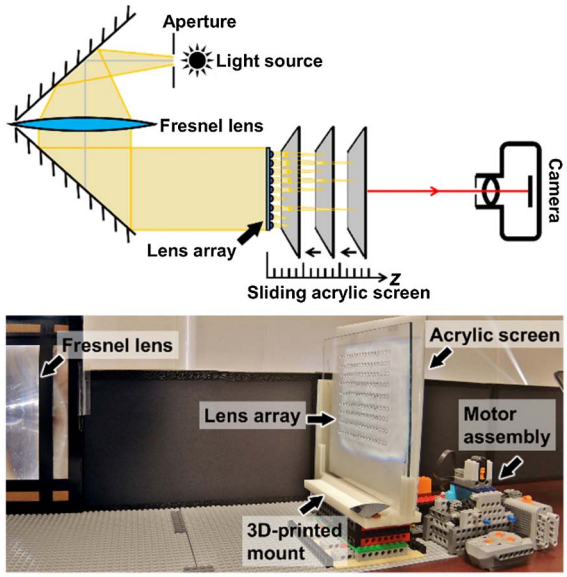

Fig. 2. Lens characterization system: A camera fixed behind the lens array allowed the outline of each lens to be imaged. With the addition of a motorized sliding acrylic screen, the light focused by each lens was projected onto the screen, and images of the projected beam profiles were captured by the camera. The system was assembled with LEGO bricks and 3D printed parts.

uniform light field produced by a high-power LED spotlight (2700 lm) with a 2 cm × 2 cm square aperture, followed by a collimating Fresnel lens ($f = 76.2$ cm) adjusted to create a collimated beam. A translucent acrylic screen placed on a motorized stage near the back focal plane of the lens array provided a surface for focused beam profiles to be projected. A camera (Nikon D5500, 24MP) was set to capture full resolution images of beam profiles at regular intervals. For diameter characterization, the sliding acrylic screen was removed and the lens array rotated to face the illumination source, which enabled the circumference of each lens to be clearly imaged.

The user-controllable motorized stage was made with LEGO components (#8881,2,4,5, #4716, #10928 #4019, #3649, #32185). The motor was powered by a battery pack and controlled by remote control via a receiver. The motor achieved continuous 90 rpm clockwise or counterclockwise motion, which translated into a horizontal displacement of acrylic screen stage. The use of worm gears, a drop-down gear system, and gear rack translated every 360° motor rotation into 0.32 mm of linear horizontal displacement at 0.5 mm/s speed. The increased torque from the drop-down gear system enabled uniform displacement throughout the entire range. The motor assembly schematic generated by Digital Designer software (LEGO) is shown in Fig. 3.

The cost of the system included ~$100 for LEGO bricks, gears, motors, plates, and electrical connectors, ~$100 for an LED spotlight and other optical components such as a large Fresnel lens and mirrors, and $10 for 3D printing costs. The most expensive components were the digital camera and computer, which together cost about $1000. In comparison, a typical lens-checking system (interferometer or profilometer) can be significantly more expensive. [8,10,11]

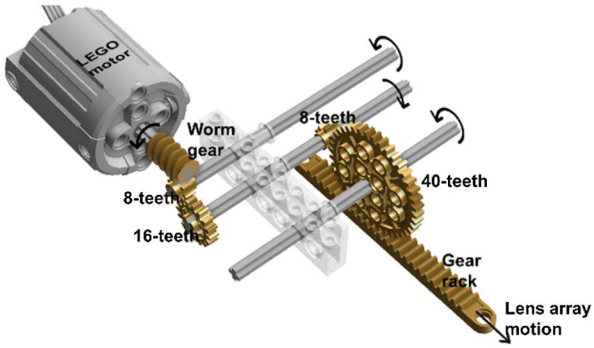

Fig. 3. LEGO motor and gear schematic.

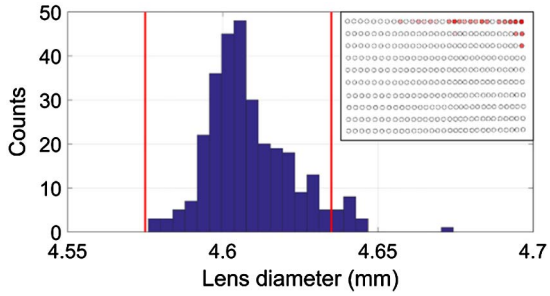

Fig. 5. Histogram of lens diameters: 283 of 300 lenses are within specifications of $d = 4.61 \pm 0.03$ mm. Inset shows a color-coded image, where lenses highlighted in red did not meet specifications.

The camera was equipped with a standard 18-55 mm $f/3.5-5.6$ lens. A 55 mm focal length was selected to minimize distortions, and an aperture of $f/8$ was selected to maximize depth-of-focus and minimize optical aberrations. The distance between the camera and substrate was 50 cm, which yielded a field of view (FOV) of 40 cm × 30 cm. The FOV was selected to yield a sampling resolution of 50 μm. By mounting the camera closer to the lens array, improved image resolution could be achieved due to increased sampling points per lens with a reduced FOV. Camera Control Pro software (Nikon) was used for remote camera shutter control from a laptop computer. The codes for image processing and analysis were written in MATLAB (MathWorks).

4. RESULTS

A 30 × 10 lens array was printed with 25 μL ± 0.2% elastomer at 210°C, as shown in Fig. 4. A US penny was placed next to the array for size calibration.

A. Diameter Characterization

Pixel size calibration was performed with a US penny affixed next to the lens array. The image was processed by MATLAB. First, the image was binarized. Second, Hough transform was used for circle detection: the coin was detected and pixel distances calibrated according to the coin diameter (19.7 mm). Subsequently, each lens was detected and its pixel coverage measured; the data were converted to an absolute distance for each lens. Lenses with a circularity <0.98 were automatically rejected. Third, a histogram of lens diameters was generated, as shown in Fig. 5. The locations and sizes of each lens were color-coded over the original image for visual inspection, as shown in Fig. 5 (inset). The program required 5 s of total execution time per image, or ~20 ms per lens.

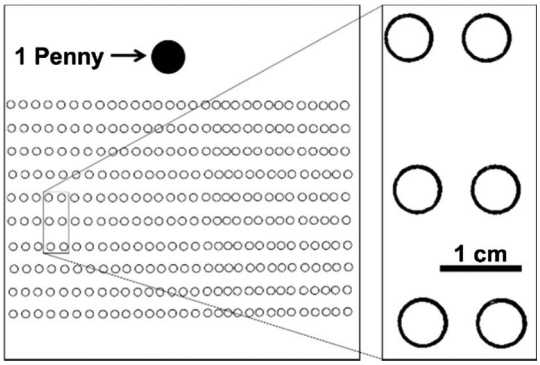

Fig. 4. Binarized image of as-printed 30 × lens array (30 × 10 lenses).

Diameter characterization concluded that 283 out of 300 lenses were within an arbitrary specification of $d = 4.61 \pm 0.03$ mm (method of obtaining specification shown in Section 5). The mean and standard deviation of the within-specification lenses were 4.61 mm and 0.01 mm, respectively, and the relative standard deviation (RSD) was 0.2%. The overlaid color map indicated that lenses near the top right perimeter printed larger than specified due to uneven heat distribution.

The inherent error in the imaging system was measured by repeating the diameter characterization process with an array of printed circles that occupied the entire image FOV. Repeated images of an array of 4.6 mm diameter circles printed by a computer printer (Brother HL-L2300D) at 2400 dpi concluded that the imaging system error was less than ±0.25% within the usable FOV (defined as a square drawn from the center that does not exceed 50% of the entire FOV in the longer dimension).

B. Focal Length Characterization

Lens focal length was determined using the same setup with the addition of a motorized sliding translucent acrylic screen attached in front of the lens array to image the projected beam profiles. To accurately characterize the focal length of each lens, the lenses were oriented backwards such that the planar sides of the lenses were on the same plane. The focal length of each lens was defined as the lens-to-screen distance when the full-width at half-maximum (FWHM) of its projected focal spot was minimized. The LEGO motor translation stage enabled the screen to slide from $z = 20$ mm to $z = 3$ mm behind the lens array (where $z = 0$) at 0.5 mm/s. The camera captured full-resolution images at 5 fps, which allowed image acquisition at every 100 μm interval in lens-to-screen distance. A higher focal length resolution could be achieved by stepping down the motor. The shutter speed was set sufficiently fast (1/120s) to prevent the projected beam intensity from saturating the camera sensor and motion blur.

For each image, the camera captured the entire array of the focal spot beam profiles. After sequential image acquisition at different z distances, the images were processed frame by frame. For a single frame, the beam profile of each lens was detected,

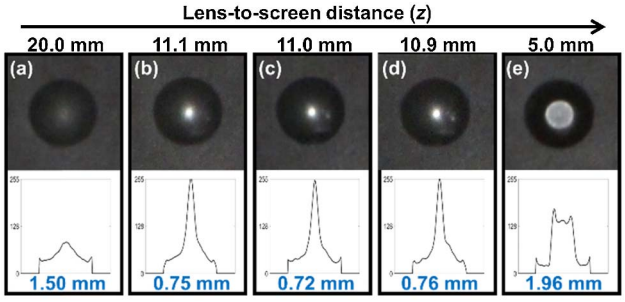

Fig. 6. Projected beam profile of a single lens at different z distances, showing raw image, x-axis intensity profile, and calculated FWHM (blue font). The focal length of this particular lens was 11.0 mm.

background subtracted, and the FWHM of the intensity profile was calculated in both the x and y directions. This generated a matrix that contained the location and FWHM for every lens in one acquired frame. The FWHM from all frames were compared, and the z distance of the corresponding frame where the FWHM reaches minimum was used as the focal length of the lens. Each image required 8 s processing time, with a total execution time for 170 frames set to roughly 20 min. However, since the focal length was known to be in the range of 11 mm, only images acquired for lens-to-screen distances within 8–14 mm were processed, thereby shortening the total processing time to 8 min. For this lens array of 300 lenses, this yielded a calculation time of 1.6 s per lens.

Figure 6 shows the projected beam profile of one lens within the array. Figures 6(a)–6(e) show the evolution of the intensity profile of the selected lens at five z distances. The FWHM was calculated in both the x and y directions, and the focal length was verified as 11.0 mm for this lens. A histogram of the focal length from all 300 lenses is shown in Fig. 7.

Focal length characterization concluded that 265 out of 300 lenses were within an arbitrary specification of $f = 11.4 \pm 1.1$ mm (method of obtaining specification shown in Section 5). The mean and standard deviation of the within-specification lenses were 11.52 mm and 0.40 mm, respectively, and the RSD was 3.4%. It was observed that the out-of-specification lenses during diameter characterization also did not meet the required focal length requirements, due to the incorrect geometry caused by uneven heat distribution.

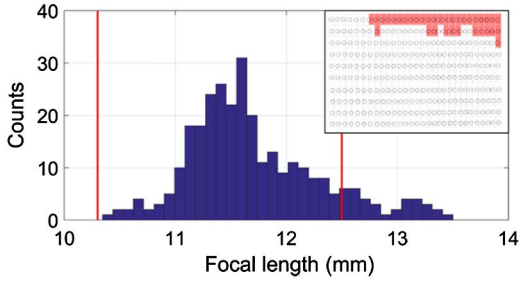

Fig. 7. Histogram of lens focal lengths: 265 of 300 lenses are within specifications of $f = 11.4 \pm 1.1$ mm. Inset shows the original image overlaid with a color map to indicate out-of-specification units.

The accuracy of focal length measurements depends on the correct distance between the lens array and screen. The distance between the acrylic screen and glass plate was verified with calipers across the entire region, and the tightly fitting 3D-printed components ensured a difference less than 100 μm. The focal lengths of randomly selected lenses were measured by a previous method [1] and compared with results obtained from the system, which yielded a difference up to 100 μm.

5. DISCUSSION

For lenses printed with the same nominal volume, e.g., 25 μL, it was observed that increased surface temperature caused the elastomer to cure faster, leading to a smaller lens diameter, as shown in Fig. 8 (solid curve). As the elastomer volume remained constant, a smaller lens diameter caused the lens to have a larger curvature and shorter focal length, as shown in Fig. 8 (dashed curve).

Both diameter and focal length depend solely on the curing temperature of the substrate for a fixed volume. Figure 9 shows the lens focal length (f_{Lens}) versus diameter (d), where an empirical calibration curve can be obtained as $f_{\text{Lens}} = 10^{-4} \times \exp^{(2.52 \times d)}$, with $R^2 = 98.5\%$.

As mentioned earlier, to avoid exhaustive testing of each lens on a smartphone with a target for magnification and resolution, it is highly desirable to establish an empirical calibration curve to relate these "performance" parameters to lens parameters such as the diameter and focal length.

The system magnification M of the smartphone microscope system is defined by comparing the image to an object of known size (USAF 1951 resolution test target). Since the perceived magnification of a smartphone microscope changes with

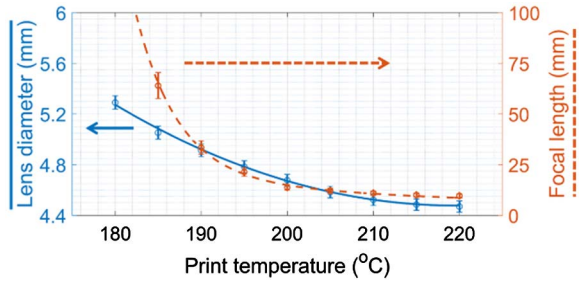

Fig. 8. Diameter and focal length of lenses printed with 25 μL (30 ×) at various temperatures.

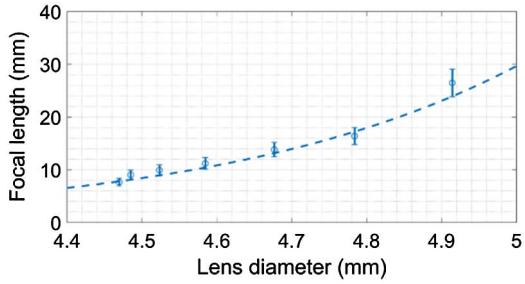

Fig. 9. Lens focal length versus. diameter for 25 μL (30 ×) lenses. A fit was found where $f_{\text{Lens}} = 10^{-4} \times \exp^{(2.52 \times d)}$.

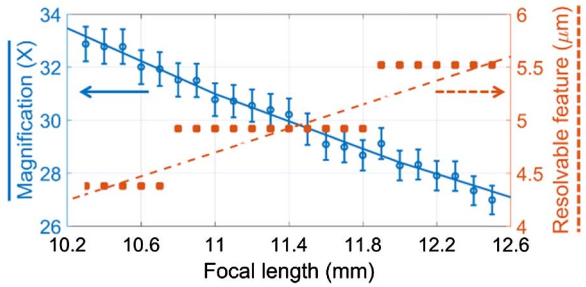

Fig. 10. Calibration chart relating focal length to its magnification and resolution. A fitting curve was found to be $M = 340.89/f_{\text{Lens}}$.

different display sizes and smartphone orientation, we followed a standard resolution baseline of 300 dpi. (This value corresponds to the minimum human eye resolution at normal reading distance of 30 cm [17]). For example, a Lumia 640 used in this work produces an image with 3264 × 2448 pixels, which is 278 mm × 208 mm at 300 dpi. For a magnification that is display independent, we could define a distance constant c, such that $M = c/f_{\text{Lens}}$, where f_{Lens} is the focal length of the elastomer lens itself. The equation is valid if the distance between the cardinal points and imager remains constant; therefore, the focusing mechanism on the Lumia 640 was fixed by software to operate at its shortest working distance.

Next, we individually obtained the magnification and minimum resolvable feature of 265 lenses that met the focal length specification (11.4±1.1 mm) in Fig. 7. As shown in Fig. 10, the focal length and magnification can be related by a fitting curve where $M = 340.89/f_{\text{Lens}}$ with $R^2 = 98.9\%$.

The smallest resolvable feature is $R = \text{FOV}/p\#$, where FOV is the dimension of the image full FOV, and p# is the number of pixels on the imaging sensor. For the Lumia 640 with a 30 × elastomer lens operated at a minimum working distance (WD) of 18 mm and FOV of 7.82 mm× 5.87 mm, a theoretical value $R = 2.40$ μm per pixel can be obtained. Experimentally, the optical resolution did not achieve the diffraction limit due to lens aberrations and RGB color filter efficiencies of the imaging sensor, among other factors. Experimental measurements yielded $R = 4.5 - 5.5$ μm for the Lumia 640 with a 30 × elastomer lens, and precisely 4.92 μm at exactly 30 ×. Despite the discontinuous distances in the resolution test images, a linear fitting curve can be obtained since the FOV of the images are known.

The fitting results suggest that the focal length of up to 300 lenses can be used to simultaneously obtain system magnification and resolution without the need for further one-by-one system-level testing, which is labor intensive and time consuming. In order to achieve magnification tolerance of 30 × ±10% and resolution better than 6 μm for the lens, the lenses were printed with 25 μL ± 0.2% volume of elastomer, and the diameter and focal length tolerances were calculated 4.61 ± 0.03 mm and 11.4 ± 1.1 mm, respectively.

6. CONCLUSION

Inkjet-printed optics enabled high-throughput and inexpensive fabrication of lenses with tunable geometry, magnification, and focal length. However, the dependence on environmental factors warrants each lens to be inspected for conformity to its nominal specifications. We have demonstrated an imaging setup assembled with off-the-shelf parts, LEGO bricks and 3D printed components, and a workflow to perform these characterizations. A diameter resolution of 50 μm and focal length resolution of 100 μm have been achieved simultaneously for up to 300 lenses. The fast image processing and minimal sample modification would enable this platform to assist in in-line inspection in manufacturing facilities.

Funding. National Science Foundation (NSF) (1151154, 1643391).

Acknowledgment. YS, WS: Dr. Shih, LLC (I, P). LEGO is a trademark of the LEGO Group of companies, which does not sponsor, authorize or endorse this activity.

REFERENCES

1. Y.-L. Sung, J. Jeang, C.-H. Lee, and W.-C. Shih, Fabricating optical lenses by inkjet printing and heat-assisted in situ curing of polydimethylsiloxane for smartphone microscopy, J Biomed. Opt. **20**, 047005 (2015).
2. R. R. Jahan-Tigh, G. M. Chinn, and R. P. Rapini, "A comparative study between smartphone-based microscopy and conventional light microscopy in 1021 dermatopathology specimens," Arch. Pathol. Lab. Med. **140**, 86–90 (2016).
3. J. C. Contreras-Naranjo, Q. Wei, and A. Ozcan, "Mobile phone-based microscopy, sensing, and diagnostics," IEEE J. Sel. Top. Quantum Electron. **22**, 1–14 (2016).
4. T. Mizuno, R. Shibata, M. Kobayashi, Y. Matsuyama, H. Ohbayashi, and M. Funakura, "Lens grinding apparatus for grinding an eyeglass lens from a plurality of directions," U.S. patent 5,716,256, 10 February 1998.
5. M. Heckele, W. Bacher, and K. Müller, "Hot embossing-the molding technique for plastic microstructures," Microsyst. Technol. **4**, 122–124 (1998).
6. W. Lee, A. Upadhya, P. Reece, and T. G. Phan, "Fabricating low cost and high performance elastomer lenses using hanging droplets," Biomed. Opt. Express **5**, 1626–1635 (2014).
7. I. Lavrador, X. Lippens, A. Chansavoir, P. Larue, D. Steigelman, L. Kabelaan, and J. F. Cailloux, "Process for controlling a lens manufacturing process," U.S. patent 8,721,076, 13 May 2014.
8. T. Shalon and M. L. Pund, "Automated lensometer," U.S. patent 5,331,394, 19 July 1994.
9. R. Biel and A. Lang-Scholl, "Lens checking apparatus," U.S. patent 6,765,661, 20 July 2004.
10. J. Duparre, "Fabrication process for mastering imaging lens arrays," U.S. patent 8,231,814, 31 July 2012.
11. M. Hori, T. Sasaki, H. Yamamoto, K. Fukuda, K. Yamada, T. Anzaki, K. Hamanaka, K. Nakamura, and M. Kido, "Optical device and method for fabricating the same," U.S. patent 7,006,291, 28 February 2006.
12. T.-H. Hsieh, Y.-C. Tsai, C.-J. Kao, Y.-M. Chang, and Y.-W. Lu, "A conceptual atomic force microscope using LEGO for nanoscience education," Int. J. Autom. Smart Technol. **4**, 113–121 (2013).
13. K. Knagge and D. Raftery, "Construction and evaluation of a LEGO spectrophotometer for student use," Chem. Educator **7**, 371–375 (2002).
14. F. Quercioli, B. Tiribilli, A. Mannoni, and S. Acciai, "Optomechanics with LEGO," Appl. Opt. **37**, 3408–3416 (1998).
15. S. A. Lee, J. Erath, G. Zheng, X. Ou, P. Willems, D. Eichinger, A. Rodriguez, and C. Yang, "Imaging and identification of waterborne parasites using a chip-scale microscope," PLoS One **9**, e89712 (2014).
16. E. Pastrana, "High-tech Petri dishes," Nat. Methods **8**, 999 (2011).
17. E. Ackerman, "Considerable material on vision from a medical point of view," in *Biophysical Science* (Prentice-Hall, 1962).